The Configuration Evolution and Macroscopic Elasticity of Fluid-filled Closed Cell Composites: Micromechanics and Multiscale Homogenization Modelling

Lianhua Ma[1], Bernard F. Rolfe[2], Qingsheng Yang[1,3] and Chunhui Yang[2,3]

Abstract: For fluid-filled closed cell composites widely distributed in nature, the configuration evolution and effective elastic properties are investigated using a micromechanical model and a multiscale homogenization theory, in which the effect of initial fluid pressure is considered. Based on the configuration evolution of the composite, we present a novel micromechanics model to examine the interactions between the initial fluid pressure and the macroscopic elasticity of the material. In this model, the initial fluid pressure of the closed cells and the corresponding configuration can be produced by applying an eigenstrain at the introduced fictitious stress-free configuration, and the pressure-induced initial microscopic strain is derived. Through a configuration analysis, we find the initial fluid pressure has a prominent effect on the effective elastic properties of freestanding materials containing pressurized fluid pores, and a new explicit expression of effective moduli is then given in terms of the initial fluid pressure. Meanwhile, the classical multiscale homogenization theory for calculating the effective moduli of a periodical heterogeneous material is generalized to include the pressurized fluid "inclusion" effect. Considering the coupling between matrix deformation and fluid pressure in closed cells, the multiscale homogenization method is utilized to numerically determine the macroscopic elastic properties of such composites at the unit cell level with specific boundary conditions. The present micromechanical model and multiscale homogenization method are illustrated by several numerical examples for validation purposes, and good agreements are achieved. The results show that the initial pressure of the fluid phase can strengthen overall effective bulk modulus but has no contribution to the shear modulus of fluid-filled closed cell composites.

---

[1] Department of Engineering Mechanics, Beijing University of Technology, Beijing 100124, PR China

[2] School o f Engineering, Deakin University, Locked Bag 20000, GEELONG VIC 3220, Australia

[3] Qingsheng Yang, Email: qsyang@bjut.edu.cn; Chunhui Yang, Email: chunhui.yang@deakin.edu.au

Keywords: Fluid-filled closed cell composites, effective properties, micromechanics, multiscale homogenization.

1 Introduction

It is well known that typical fluid-filled closed cell composite is a kind of porous material. In general, porous materials can contain isolated closed voids or interconnected open cell structures (Gibson et al, 1997), such as saturated rocks, salt water ice, polymer foams, plant cells and biological tissues. The existences of voids and fluids at the micro-scale have significant influences on macroscopic mechanical properties of porous materials. In typical open cell porous media, the fluid in pores can flow from one pore to the others. In the past decades, numerous studies have been devoted to the macroscopic properties of such porous materials. The specific nature of mechanical behavior of the fluid-saturated porous media was recognized early in poromechanics developed by Biot (Biot, 1954). Ever since, poromechanics and effective medium theory have entered a large number of engineering applications, ranging from traditional geophysical field to biomechanical engineering. Many investigations on their effective properties of fluid-saturated porous media have been reported (Budiansky and O'Connell, 1976; Coussy, 1995; Dormieux et al., 2006).

It is noted that the classical poroelasticity is mostly restricted to open-cell porous materials, where the fluids can freely flow through open pores and can be squeezed out in deformations. However, for some unique fluid-filled closed cell materials, such as metal foams filled with fluids (Ozgur et al.,1996), closed cell rocks, foamed polymers, plant cells and carrot tissues (Kimmel, 1992; Warner et al, 2000), it is well accepted that the structure of the fluid-filled closed cell material resembles that of a closed cell impermeable solid filled with a pressurized liquid. For example, in carrot tissue, the turgor can induce the overall deformation of the tissue, and the experimental results show that turgor pressure plays a major role in the macroscopic elasticity of the carrot tissue (Georget, 2003). Several investigations of effective properties of materials with closed fluid-filled pores have been reported. O'Connell and Budiansky (O'Connell and Budiansky, 1974, 1976) examined the effective elastic properties of fluid-filled materials with different geometries of pores. The fluid pressure polarization phenomenon was addressed by Zimmerman (1991). Kachanov et al. (Kachanov, Shafiro et al, 1993-1997) considered an arbitrary orientational distribution of crack-like cavities, the fluid pressure polarization and the impact of fluid on stress interactions on cracks. In addition to these micromechanics methods, some experimental observations and numerical simulations have also been done on the effective elastic behaviors of fluid-filled closed cell material, especially of plant materials. In the field of botany, the typical

plant and food materials are usually treated as a special kind of fluid-filled closed cell composites. A model of a liquid filled closed cell structure was used to examine the effective elasticities of plant materials such as potatoes (Nilsson, 1958), carrot tissues (Georget et al., 2003) and yeast cells (Stenson et al., 2009). For these unique fluid-filled materials, the experimental measurements show that the overall elastic moduli increase linearly with initial fluid pressure. In the aspect of numerical modeling, Cheng et al (1987) developed a finite element model to simulate the mechanical deformations of cells and embryos. Ozgur et al. (1996) used a specialized finite element program to model the effective mechanical behaviors of closed cell metal composites filled with hydrostatic fluids. Smith et al. (1998) also used a finite element approach to extract the elastic properties of plant cells, but introduced the possibility of permeable cell walls. Hartmann et al. (2004, 2006) numerically modeled the compression deformation of a yeast cell subjected to high hydrostatic pressure, where it is assumed that the cytoplasm behaves like pure fluid. Zhang, Lv and Zheng (2010) reported an extended multiscale finite element method for modeling the mechanical analysis of closed liquid cell materials. In their work, a higher order coarse-grid element was constructed to characterize the mechanical deformations of such materials with greater accuracy. Huang et al. (2011) developed a boundary element technique to solve the elastic problems of 2D closed solids with many fluid-filled pores of various shapes. Although numerical studies can yield accurate results in some occasions, only limited circumstances were modeled with specific geometries of pores.

In previous models, the effect of initial fluid pressure and configuration evolution were not fully considered. Actually, for typical freestanding closed cell materials filled with pressurized fluids, there are initial pressures in closed cells. The initial pressures can induce residual stresses in pore/matrix phase and also cause initial macroscopic deformations leading to configuration change of such materials. The main purpose of this paper is to develop an analytical micromechanics model and an asymptotic homogenization-based finite element model for the problems of closed-cell composites containing pressurized fluid-filled pores, and to investigate the effective properties of such materials. The major addressed issue in this paper is the treatment of the initial pressure and closed fluid inclusions in the composites. Three different configurations are firstly introduced to facilitate the effect of initial fluid pressure, and then the fluid-pressure induced initial macroscopic strains can be determined by the proposed micromechanics method and the multiscale homogenization model. Based on the configuration evolution and the derived initial macroscopic strains, the effective elastic properties of such materials in initial state can be further obtained by the present models.

The contents of this paper are organized in five major sections. The microme-

chanical model of fluid-filled closed cell materials is described, and explicit expressions of effective properties for closed cell porous composites with inner fluid pressures are derived in Section 2. The multiscale homogenization-based method for macroscopic behavior and micromechanical deformations of solids containing periodical fluid-filled pores are given in Section 3, where the periodical boundary conditions of a unit cell subjected to internal pressures are presented. In Section 4, the proposed models are applied to analyze the overall elastic stiffness of fluid-filled closed-cell composites. The effects of fluid pressure, bulk modulus and pore shape on effective properties are then discussed in detail. Section 5 summarizes the conclusions and future work based on the results obtained..

2   Micromechanics of fluid-filled closed cell composites

The equivalent inclusion model is one of the effective methods for estimating a homogenized elastic property of composite materials. It was originally used for the determination of effective properties of composites containing solid inclusions. In this section, an equivalent inclusion method based on the Mori-Tanaka model (Mori and Tanaka, 1972) is extended to the composites containing fluid-filled pores.
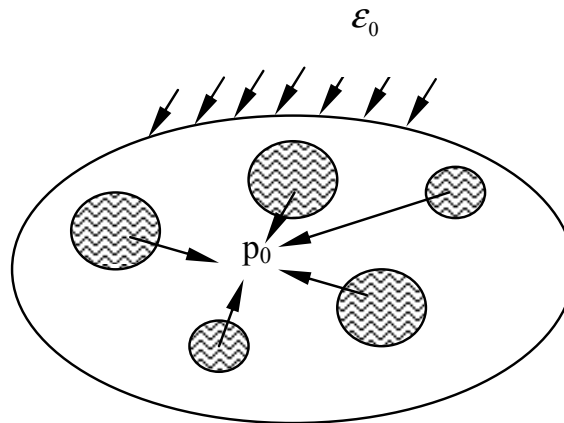

Figure 1: The representative volume element (RVE) of fluid-filled closed-cell composites subjected to pore pressure p_0 and macroscopic strain ε_0

The Representative Volume Element (RVE) of a closed-cell material with a sufficiently large number of pores is chosen, as shown in Figure 1, with an arbitrary distribution of pores. For the solid containing fluid-filled pores, the solid phase is assumed to be linear elastic and impermeable, and the pore space is filled with a

fluid at a pressure p, which is identical in all pores. The fluid phases in the composites can be represented as an equivalent isotropic elastic solid, with the shear modulus $\mu_f = 0$. Therefore, the compression stiffness tensor of the pore can be given as,

$$C_{ijkl}^f = k_f \delta_{ij} \delta_{kl} \tag{1}$$

where δ_{ij} is the Kronecker delta function, k_f is the bulk modulus of the fluid. Throughout the present paper, Einstein's summation convention over the repeated indices is satisfied. If the material is subjected to tension loads, the pore is equivalent to the cavity without fluid. Thus its bulk modulus reduces to zero and the corresponding elastic stiffness tensor becomes zero tensor $C_{ijkl}^f = 0$.

2.1 Micromechanical model without initial fluid pressures

To simplify the derivation, the case of the fluid pressure-free is firstly considered. According to Eshelby's equivalent inclusion theory (Eshelby, 1957), an eigenstrain ε^* for a particular pore can be calculated by embedding the pore into the matrix. It is assumed that a uniform stress is applied at infinity, the induced internal stress in the pore domain can be expressed as,

$$P_{ij} = C_{ijkl}^f \left(\bar{\varepsilon}_{kl}^s + S_{klmn} \bar{\varepsilon}_{mn}^* \right) = C_{ijkl}^s \left(\bar{\varepsilon}_{kl}^s + S_{klmn} \bar{\varepsilon}_{mn}^* - \bar{\varepsilon}_{kl}^* \right) \tag{2}$$

where P_{ij} is the internal pore stress, $\bar{\varepsilon}_{ij}^s$ is the average elastic strain in the matrix, C_{ijkl}^s is the stiffness tensor of the matrix, S_{ijkl} is the Eshelby's tensor depending on pore shape and elastic properties of the matrix, $\bar{\varepsilon}_{ij}^*$ is the hypothetic eigenstrain in the equivalent inclusions caused by the presence of the pore replacing matrix material.

Gassmann (1951) and Brown et al. (1975) have shown that pore pressure, p_f, can be calculated from the total change of pore volume for compressive loading. Mathematically it has the form,

$$p_f = -k_f \frac{\delta V_p}{V_p} \tag{3}$$

where $\delta V_p / V_p$ is the normalized pore volume change, which can be expressed by the sum of total normal strains,

$$\frac{\delta V_p}{V_p} = \bar{\varepsilon}_{ii}^s + S_{iikl} \bar{\varepsilon}_{kl}^* \tag{4}$$

The pore stress, P_{ij}, is then given by,

$$P_{ij} = -p_f \delta_{ij} \tag{5}$$

Because the fluid in pores cannot bear tensile and shear loads, each component of the elastic stiffness tensor remains zero when the material is subjected to tensile or shear load.

According to the Mori-Tanaka model (Mori and Tanaka, 1972), for the fluid-filled closed-cell materials without initial pore pressure, the effective elastic stiffness is thus written as,

$$\bar{C}_{ijkl} = \left(\varphi_s C^s_{ijmn} I_{mnpq} + \varphi_f C^f_{ijmn} \tilde{A}_{mnpq} \right) \left(\varphi_s I_{pqkl} + \varphi_f \tilde{A}_{pqkl} \right)^{-1} \qquad (6)$$

where I_{ijkl} is the identity tensor; ϕ_s and ϕ_f are the volume fraction of the solid matrix and closed pores, respectively, with $\phi_s + \phi_f = 1$, and $\tilde{A}_{ijkl}$ is defined by

$$\tilde{A}_{ijkl} = \left[I_{ijkl} + S_{ijmn} \left(C^s_{mnpq} \right)^{-1} \left(C^f_{pqkl} - C^s_{pqkl} \right) \right]^{-1} \qquad (7)$$

In particular, as the pore is spherical, the Eshelby's tensor is isotropic, and the effective properties of the composites can be characterized by the effective bulk modulus $\bar{K}$ and shear modulus $\bar{G}$,

$$
\begin{aligned}
\bar{K} &= k_m \left(1 + \frac{\varphi_f \left(k_f - k_m \right)}{\alpha \left(1 - \varphi_f \right) \left(k_f - k_m \right) + k_m} \right), \quad \alpha = \frac{1 + v_m}{3 \left(1 - v_m \right)} \\
\bar{G} &= \mu_m \left(1 + \frac{\varphi_f}{\beta \left(1 - \varphi_f \right) - 1} \right), \quad \beta = \frac{2 \left(4 - 5 v_m \right)}{15 \left(1 - v_m \right)}
\end{aligned}
\qquad (8)
$$

where v_m, k_m and μ_m are the Poisson's ratio, bulk and shear modulus of the solid matrix, respectively. When the pores are subjected to tension load, the overall properties are equivalent to those of closed-cell porous materials, and Eq. (8) can be reduced to the results of Tandon and Weng (1988).

It is worth noting that the macroscopic moduli of such materials can also be estimated by other well-developed methods, for example, the dilute scheme, the self-consistent method (Hill, 1965), and the generalized self-consistent method (Christensen and Lo, 1979).

2.2 *Micromechanical analysis of closed cell solids with initial fluid pressures*

Now let us consider the effective properties of the materials with a given initial fluid pressure. As mentioned above, in the initial state of the closed cell materials with fluid-filled pores, the pore domain is pressurized by a fluid pressure. Accordingly, the solid matrix is also initially prestressed for the whole material in order to be self-equilibrated. For the macroscopic elasticity of solids containing initial residual stress, it is essential to introduce a fictitious stress-free configuration to examine the elastic stresses and strains in both solid and fluid phase.
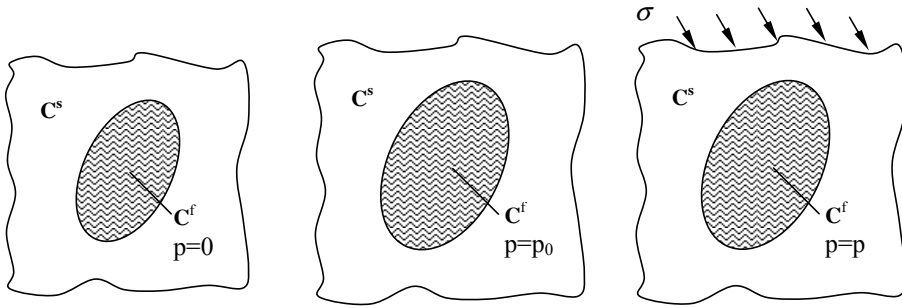
(a) Fictitious stress-free configuration   (b) Initial configuration   (c) Current configuration

Figure 2: The evolution of micromechanical model for a fluid-filled closed-cell composite described by three configurations

For convenience, we define the following terminology to describe the three configurations of the RVE: the fictitious stress-free configuration, the initial configuration, and the current configuration. The fictitious stress-free configuration refers to the imaginary zero-stress state of both the solid phase and the pores, which can be obtained by hypothetically releasing the initial pressure in the fluid pores, and having the fluid pore and solid matrix return to their stress-free state. The so-called fictitious stress-free configuration was first introduced by Sun, Huang et al (2004, 2006) to study the elastostatic problems of multi-phase material involving surface/interface energy effects. Based on the fictitious stress-free configuration concept, we apply the initial pressure on the fluid in the pores and thus the solid matrix will deform until a new equilibrium state is reached, which is the initial configuration where the material does not experience any external load. It should be pointed out that the initial elastic field in this configuration is compatible. This is entirely due to the existence of the initial fluid pressure. When an additional external load is applied on the initial configuration, the RVE will further deform and reach to a new equilibrium configuration, which is defined as the current configuration. Figure 2 illustrates the evolution of three configurations for the RVE of a fluid-filled closed cell material. The fictitious stress-free configuration introduced here can be used to characterize the local average strains of the material and to deduce the initial macroscopic strains. Considering the similar configuration evolutions, Zhang et al (2009) proposed a micromechanics model to investigate the effects of gas pressure on the macroscopic elastoplastic properties of porous materials.

At the fictitious stress-free configuration, we can apply another extra eigenstrain,

$\tilde{\varepsilon}_{ij}^{p0}$, on the pores to produce an initial fluid pressure. In such case, the internal pore stress can be written as,

$$P_{ij}^0 = C_{ijkl}^f \left(\tilde{\varepsilon}_{kl}^s + \tilde{\varepsilon}_{kl}^f - \tilde{\varepsilon}_{kl}^{p0} \right) = C_{ijkl}^s \left(\tilde{\varepsilon}_{kl}^s + \tilde{\varepsilon}_{kl}^f - \tilde{\varepsilon}_{kl}^* - \tilde{\varepsilon}_{kl}^{p0} \right) \tag{9}$$

where P_{ij}^0 is the initial pore stress related to initial pore pressure by $P_{ij}^0 = -p_0 \delta_{ij}$, $\tilde{\varepsilon}_{ij}^s$ is the initial average strain in the matrix produced by initial pore pressure, $\tilde{\varepsilon}_{ij}^*$ is the hypothetic eigenstrain in the equivalent inclusions, and $\tilde{\varepsilon}_{ij}^f$ is referred to as the average perturbing strain in the fluid phase, which is related to $\tilde{\varepsilon}_{ij}^*$ and $\tilde{\varepsilon}_{ij}^{p0}$ as follows,

$$\tilde{\varepsilon}_{ij}^f = S_{ijkl} \left(\tilde{\varepsilon}_{kl}^* + \tilde{\varepsilon}_{kl}^{p0} \right) \tag{10}$$

In addition, self-equilibrium of the fluid-filled composites in the initial state leads to,

$$(1 - \varphi_f) \left(C_{ijkl}^s \tilde{\varepsilon}_{kl}^s \right) + \varphi_f P_{ij}^0 = 0 \tag{11}$$

Combining Eq.(9) and Eq.(11), we have

$$\tilde{\varepsilon}_{ij}^s + \varphi_f \left(\tilde{\varepsilon}_{ij}^f - \tilde{\varepsilon}_{ij}^* - \tilde{\varepsilon}_{ij}^{p0} \right) = 0 \tag{12}$$

And substituting Eq. (10) into Eq. (12) gives

$$\tilde{\varepsilon}_{ij}^s = -\varphi_f \left(S_{ijkl} - I_{ijkl} \right) \left(\tilde{\varepsilon}_{kl}^* + \tilde{\varepsilon}_{kl}^{p0} \right) \tag{13}$$

Using Eq.(10), we have

$$\tilde{\varepsilon}_{ij}^f = \frac{1}{\varphi_f} \left[\left(S_{ijkl} \right)^{-1} - I_{ijkl} \right]^{-1} \tilde{\varepsilon}_{kl}^s \tag{14}$$

The initial strain of solid phase $\tilde{\varepsilon}_{ij}^s$ can be easily obtained by Eq.(11)

$$\tilde{\varepsilon}_{ij}^s = -\frac{\varphi_f}{1 - \varphi_f} \left(C_{ijkl}^s \right)^{-1} P_{kl}^0 \tag{15}$$

The induced initial macroscopic strain of the composite with respect to the fictitious stress-free configuration can be written as,

$$\bar{\varepsilon}_{ij}^0 = (1 - \varphi_f) \tilde{\varepsilon}_{ij}^s + \varphi_f \left(\tilde{\varepsilon}_{ij}^s + \tilde{\varepsilon}_{ij}^f \right) \tag{16}$$

Substituting Eq. (14) and (15) into Eq.(16), and after some algebraic operations, the initial macroscopic strain $\bar{\varepsilon}_{ij}^0$ can be simply expressed by

$$\bar{\varepsilon}_{ij}^0 = -\frac{\varphi_f}{1-\varphi_f} \left(I_{ijkl} - S_{ijkl}\right)^{-1} \left(C_{klmn}^s\right)^{-1} P_{mn}^0 \tag{17}$$

As seen from Eq.(17), the produced initial macroscopic strain, $\bar{\varepsilon}_{ij}^0$, can be determined by the initial pore pressure and the properties of the solid matrix.

To determine the effective stiffness of the material with respect to the initial configuration, we apply a uniform stress, σ_{ij}, at infinity and then get the current configuration of the RVE, as shown in Figure 2(c). Because the initial strains exist in the initial configuration, the overall stress-strain relationship in the current configuration can be expressed as a function of the initial strain $\bar{\varepsilon}_{ij}^0$

$$\sigma_{ij} = \bar{C}_{ijkl}^0 \left(\varepsilon_{kl} - \bar{\varepsilon}_{kl}^0\right) \tag{18}$$

where ε_{ij} is the uniform strain from the fictitious stress-free configuration to the current configuration, and the effective stiffness $\bar{C}_{ijkl}^0$ can be determined by Eq.(6).

It is emphasized that, in Eq(18), both ε_{ij} and $\bar{C}_{ijkl}^0$ are with respect to the fictitious stress-free configuration. In reality, only the initial and current configurations may be experienced, and the introduced fictitious stress-free configuration is just used to produce the initial pore pressure and initial matrix stress. Although, in continuum mechanics, any configuration can be chosen as a reference configuration, yet for the sake of convenient measurement and simplicity, the initial configuration will be specifically taken as the reference configuration. Therefore, the problem becomes a determination of the effective stiffness with respect to the initial configuration.

Introducing the uniform strain, ε_{ij}', of the material from the initial configuration to the current configuration, Eq.(18) can be then expressed as,

$$\sigma_{ij} = \bar{C}_{ijkl}' \varepsilon_{kl}' \tag{19}$$

where C_{ijkl}' is the corresponding effective stiffness with respect to the initial configuration. The uniform strain ε_{ij}' with respect to the initial configuration can be related to ε_{ij} using the pressure-induced initial strain $\bar{\varepsilon}_{ij}^0$ with respect to the fictitious stress-free configuration,

$$\varepsilon_{ij} - \bar{\varepsilon}_{ij}^0 = \Lambda_{ijkl} \varepsilon_{kl}' \tag{20}$$

where Λ_{ijkl} is fourth-order tensor, and it's non-zero components are expressed as

$$\begin{array}{lll} \Lambda_{1111} = 1 + \bar{\varepsilon}_{11}^0, & \Lambda_{2222} = 1 + \bar{\varepsilon}_{22}^0, & \Lambda_{3333} = 1 + \bar{\varepsilon}_{33}^0 \\ \Lambda_{2323} = 1 + \bar{\varepsilon}_{23}^0, & \Lambda_{1313} = 1 + \bar{\varepsilon}_{13}^0, & \Lambda_{1212} = 1 + \bar{\varepsilon}_{12}^0 \end{array} \tag{21}$$

Combining Eq.(18), (19) and (20), we have

$$\bar{C}'_{ijkl} = \bar{C}^0_{ijmn}\Lambda_{mnkl} \tag{22}$$

According to Eq.(17), the initial pressure can only produce initial volumetric or normal strain of the RVE, and the initial shear strains are zero due to the pressurized fluid not being able to resist shear deformation. In other words, every solution of $\bar{\varepsilon}^0_{ij}$ is such that the shear components $\bar{\varepsilon}^0_{ij} (i \neq j)$ are zero. Particularly if the pressure in closed cells is free in the initial configuration, each component of $\bar{\varepsilon}^0_{ij}$ is zero. In this situation, Eq. (22) can be degenerated to Eq.(6). It can be observed that the fluid pressure-induced initial macroscopic strain plays an important role in determining the effective moduli with respect to the initial state.

It is noted that the micromechanical models only analytically capture macroscopic properties of both arbitrary and periodic structures, but cannot directly characterize microscopic inhomogeneous deformations.

3   Multiscale model based on asymptotic homogenization method

For heterogeneous materials composed of a periodic array of microscopic unit cells, alternative approach to predict their effective properties is the multiscale asymptotic expansion homogenization method developed in the 1970s and early 1980s (Benssousan et al., 1978; Lions, 1981). As a systematically mathematical approach, the asymptotic homogenization method has been successfully applied in the estimation of the effective material properties of composites (Bakhvalov and Panasenko, 1984; Hassani and Hinton, 1998; Okada, Fukui and Kumazawa, 2004; Yang and Becker, 2004; Haasemann, Kastner and Ulbricht, 2006). Compared the micromechanical model presented in Section 2, the asymptotic homogenization theory provides us two sets of partial differential equations at two length scales: one is the microscopic equation to be solved by using a microscopic unit cell; and the other is the macroscopic one to be solved for unknown macroscopic components. By solving these equations, predictions of the macroscopic or homogenized properties based on a periodic microstructural unit cell and calculations of microscopic and macroscopic stresses can be achieved simultaneously. Although the multiscale homogenization theory was widely employed to determine the effective properties of periodical composites, no application for liquid filled composite was reported. This section is devoted to the derivation of the effective coefficients for solids containing periodic fluid-filled pores. The governing equations for both solid and pore are obtained by using the method of multiscale expansions in the context of the asymptotic homogenization theory.

3.1 *Effective properties of periodic composites with fluid-filled pores*

Consider a closed cell composite with periodic pores without any initial hydraulic fluid pressure as depicted in Figure 3, Ω corresponds to the domain of the overall fluid-filled composite in the three-dimensional space occupied by the medium, Γ is the boundary of Ω, Y is the open subset of a space occupied by a basic unit cell, which can be divided into a solid phase Y_1 and a fluid phase Y_2 to describe the periodic microstructure of a fluid-filled composite. In real heterogeneous materials, the size of a unit cell is typically very small and can be represented by a ratio defined by $\eta = l/L$, where l is the characteristic length of the unit cell and L is that of the macroscopic region as shown in Figure 3. Hereby, two distinct length scales, i.e., the macroscopic scale x and the microscopic one y are introduced, with a relation of $y = x/\eta$.

(a) Global configuration   (b) Periodic structure of a composite   (c) Unit cell or RVE
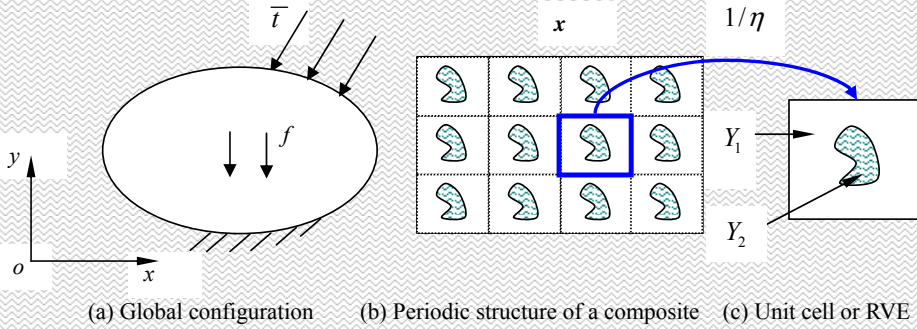
Figure 3: Characteristic dimensions of a fluid-filled closed-cell composite at two scales.

A high level of heterogeneity in the microstructure causes a rapid variation of evolutionary variables, e.g., deformations and stresses in a small neighborhood of the macroscopic scale x with a Y-periodicity. This corresponds to a microscopic scale y and consequently, all variables are assumed dependent on the small parameter η, i.e.

$$\Phi^\eta = \Phi(x, x/\eta) \tag{23}$$

Using the chain rule on differentiation,

$$\frac{\partial \Phi^\eta(x)}{\partial x_i} = \frac{\partial \Phi(x,y)}{\partial x_i} + \frac{1}{\eta} \frac{\partial \Phi(x,y)}{\partial y_i} \tag{24}$$

where the superscript η denotes the association of the function $\Phi\,(x, y)$ with the two length scales x and y. In this notation, the governing equations in different domains occupied by elastic solid phase and hydraulic fluid phase are respectively given as

$$\frac{d\sigma_{ij}^\eta}{dx_j} + f_i = 0 \qquad in\ Y_1^\eta \tag{25}$$

$$\sigma_{ij}^\eta = C_{ijkl}^\eta \varepsilon_{kl}^\eta \qquad in\ Y_1^\eta \tag{26}$$

$$\varepsilon_{kl}^\eta = \frac{1}{2}\left(\frac{\partial u_k^\eta}{\partial x_l} + \frac{\partial u_l^\eta}{\partial x_k}\right) \qquad in\ Y_1^\eta \tag{27}$$

$$\frac{dp^\eta}{dV^\eta} + \frac{\rho_R k_f^\eta}{m} = 0 \qquad in\ Y_2^\eta \tag{28}$$

$$p^\eta = -k_f^\eta \varepsilon_v^\eta \qquad in\ Y_2^\eta \tag{29}$$

where σ_{ij}^η, C_{ijkl}^η and f_i is the stress tensor, the tensor of elastic constants and body force of solid phase, respectively, and V^η denotes the deformed volume of pores when subject to compression load, p^η is the corresponding pressure field in pores, ρ_R is the reference fluid density at zero pressure, m is the total fluid mass in the pore, and ε_v^η is the volumetric compression strain of the fluid. For the closed pore subjected to compression load, a change δdV^η of the fluid volume dV^η can be expressed as

$$\varepsilon_v^\eta = \frac{\delta dV^\eta}{dV^\eta} = \frac{d\delta V^\eta}{dV^\eta} \qquad in\ Y_2^\eta \tag{30}$$

In the construction of the homogenization theory, the displacements u^η and the change of fluid volume δV^η are assumed as asymptotic expansions with respect to η

$$u_i^\eta(x) = u_i^0(x,y) + \eta u_i^1(x,y) + \eta^2 u_i^2(x,y) + \cdots, y = x/\eta \quad in\ Y_1^\eta \tag{31}$$

$$\delta V^\eta(x) = \delta V^0(x,y) + \eta \delta V^1(x,y) + \eta^2 \delta V^2(x,y) + \cdots, y = x/\eta \quad in\ Y_2^\eta \tag{32}$$

where each term of which is a periodic function with respect to y. Applying Eq.(24) to the partial differentials of strain-displacement given by Eq.(27) and stress-strain relations described in Eq.(26) of solid matrix yields,

$$\varepsilon_{ij}^\eta = \frac{1}{\eta}\varepsilon_{ij}^{-1}(x,y) + \varepsilon_{ij}^0(x,y) + \eta \varepsilon_{ij}^1(x,y) + \cdots \quad in\ Y_1^\eta \tag{33}$$

where

$$\varepsilon_{ij}^{-1}(x,y) = \frac{1}{2}\left(\frac{\partial u_i^0}{\partial y_j} + \frac{\partial u_j^0}{\partial y_i}\right) \tag{34}$$

$$\varepsilon_{ij}^0(x,y) = \frac{1}{2}\left[\left(\frac{\partial u_i^0}{\partial x_j} + \frac{\partial u_j^0}{\partial x_i}\right) + \left(\frac{\partial u_i^1}{\partial y_j} + \frac{\partial u_j^1}{\partial y_i}\right)\right] \tag{35}$$

$$\varepsilon_{ij}^1(x,y) = \frac{1}{2}\left[\left(\frac{\partial u_i^1}{\partial x_j} + \frac{\partial u_j^1}{\partial x_i}\right) + \left(\frac{\partial u_i^2}{\partial y_j} + \frac{\partial u_j^2}{\partial y_i}\right)\right] \tag{36}$$

The elastic coefficients C_{ijkl} are the periodic functions of x and depend on η and thus $C_{ijkl}^\eta = C_{ijkl}(x/\eta)$.

The stress of solid matrix can be written as

$$\sigma_{ij}^\eta = \frac{1}{\eta}\sigma_{ij}^{-1}(x,y) + \sigma_{ij}^0(x,y) + \eta\sigma_{ij}^1(x,y) + \cdots \quad in\ Y_1^\eta \tag{37}$$

where

$$\sigma_{ij}^n(x,y) = C_{ijkl}^\eta \varepsilon_{kl}^n(x,y), \quad n = -1,0,1,... \tag{38}$$

From Eqs.(35) and (37), we have

$$\sigma_{ij}^0 = C_{ijkl}^\eta\left(\frac{\partial u_k^0}{\partial x_l} + \frac{\partial u_k^1}{\partial y_l}\right) \quad in\ Y_1^\eta \tag{39}$$

Substituting Eqs. (34)-(36) for the expansion of σ_{ij}^η into Eq.(25) and equating the powers of η results in the following set of equations

$$\frac{\partial \sigma_{ij}^{-1}}{\partial y_j} = 0, \quad \frac{\partial \sigma_{ij}^{-1}}{\partial x_j} + \frac{\partial \sigma_{ij}^0}{\partial y_j} = 0, \quad \frac{\partial \sigma_{ij}^0}{\partial x_j} + \frac{\partial \sigma_{ij}^1}{\partial y_j} + f_i = 0 \quad in\ Y_1^\eta \tag{40}$$

Then integrating Eq. (40) and applying the divergence theorem to the integral in Y_1 give that u_i^0 is a function of x only, and u_i^1 can be expressed in the form

$$u_i^1 = -\Phi_i^{kl}(x,y)\frac{\partial u_k^0}{\partial x_l} \quad in\ Y_1^\eta \tag{41}$$

where Φ_i^{kl} is an unknown third order Y-periodic characteristic tensor.

Substituting Eq.(41) into Eq.(39) yields

$$\sigma_{ij}^0 = \left(C_{ijkl}^\eta - C_{ijmn}^\eta \frac{\partial \Phi_m^{kl}}{\partial y_n} \right) \frac{\partial u_k^0}{\partial x_l} \quad in \ Y_1^\eta \tag{42}$$

For the subset of fluid domain Y_2^η, introducing Eq.(32) into Eq.(30) and using Eq.(24), we have

$$\varepsilon_v^\eta = \frac{1}{\eta} \varepsilon_v^{-1}(x,y) + \varepsilon_v^0(x,y) + \eta \varepsilon_v^1(x,y) + \cdots \quad in \ Y_2^\eta \tag{43}$$

where

$$\varepsilon_v^{-1}(x,y) = \frac{\partial \delta V^0}{\partial y} \tag{44}$$

$$\varepsilon_v^0(x,y) = \frac{\partial \delta V^0}{\partial x} + \frac{\partial \delta V^1}{\partial y} \tag{45}$$

$$\varepsilon_v^1(x,y) = \frac{\partial \delta V^1}{\partial x} + \frac{\partial \delta V^2}{\partial y} \tag{46}$$

Substituting Eq.(43) into Eq.(29), the fluid pressure of the pore is given by

$$p^\eta = \frac{1}{\eta} p^{-1}(x,y) + p^0(x,y) + \eta p^1(x,y) + \cdots \quad in \ Y_2^\eta \tag{47}$$

where

$$p^n(x,y) = -k_f^\eta \varepsilon_v^n(x,y), \quad n = -1, 0, 1, \dots \tag{48}$$

From Eq.(45) and Eq.(48), we obtain

$$p^0 = -k_f^\eta \left(\frac{\partial \delta V^0}{\partial x} + \frac{\partial \delta V^1}{\partial y} \right) \quad in \ Y_2^\eta \tag{49}$$

Considering the analogy with u_i^0, both of the functions δV^0 and p^0 only depend on $\boldsymbol{x}$.

Similarly to Eq.(41), the function δV^1 takes the form

$$\delta V^1 = -\psi(x,y) \frac{\partial \delta V^0}{\partial x} \quad in \ Y_2^\eta \tag{50}$$

where ψ is another characteristic function of the terms inside the fluid domain.

Further from Eqs.(49) and (50),

$$p^0 = -k_f^\eta \left(1 - \frac{\partial \psi}{\partial y}\right) \frac{\partial \delta V^0}{\partial x} \quad in \ Y_2^\eta \tag{51}$$

Because the hydrostatic fluid in the pore cannot resist any shear deformation, the pore stresses, P_{ij}^0, is taken as the form

$$P_{ij}^0 = -p^0 \delta_{ij} \quad in \ Y_2^\eta \tag{52}$$

Then integrating on the whole domain Y leads to the homogenized stress of the unit cell subjected to an external compression load

$$\bar{\sigma}_{ij}^0 = \frac{1}{|Y|} \left(\int_{Y_1} \sigma_{ij}^0 dY_1 + P_{ij}^0 |Y_2|\right) = \overline{C}_{ijkl} \frac{\partial u_k^0}{\partial x_l} \quad in \ Y^\eta \tag{53}$$

Introducing Eqs.(42) and (52) into Eq.(53) and taking Eq.(47) into account, we have

$$\overline{C}_{ijkl} \frac{\partial u_k^0}{\partial x_l} = \frac{1}{|Y|} \int_{Y_1} \left(C_{ijkl}^\eta - C_{ijmn}^\eta \frac{\partial \Phi_m^{kl}}{\partial y_n}\right) \frac{\partial u_k^0}{\partial x_l} dY_1 + \varphi_f k_f^\eta \left(1 - \frac{\partial \psi}{\partial y}\right) \frac{\partial \delta V^0}{\partial x} \delta_{ij} \tag{54}$$

where ϕ_f is the volume fraction of the fluid phase in the unit cell space.

In the homogenization theory, $\frac{\partial u_k^0}{\partial x_l}$ and $\frac{\partial \delta V^0}{\partial x}$ characterize the unidirectional initial strain of the solid and the initial volumetric strain of the pore fluid, respectively. If they are both set to unit values, i.e. $\frac{\partial u_k^0}{\partial x_l} = \frac{\partial \delta V^0}{\partial x} = 1.0$, we can then obtain the effective elastic tensor of the composite from Eq.(54)

$$\overline{C}_{ijkl} = \frac{1}{|Y|} \int_{Y_1} \left(C_{ijkl}^\eta - C_{ijmn}^\eta \frac{\partial \Phi_m^{kl}}{\partial y_n}\right) dY_1 + \varphi_f k_f^\eta \left(1 - \frac{\partial \psi}{\partial y}\right) \delta_{ij} \tag{55}$$

Noted that Eq.(55) is only applicable for calculating the effective compression tensor. In fact, since the fluid cannot resist tensile deformation, the corresponding effective elastic tensor under tension can be determined by simply eliminating the last term of Eq.(55).

The characteristic functions Φ and ψ in Eq.(55) can be numerically determined by using a standard finite element discretization with specific boundary conditions (Wang et al., 2006). For the structure containing hydrostatic fluids, we used hydrostatic fluid elements provided by a commercial finite element analysis package–Abaqus to calculate fluid pressures and deformed volumes. These elements provide the coupling between the deformation of the fluid-filled structure and the pressure

exerted by the contained fluid along the boundary of the pore. The fluid volume, $\bar{V}$, derived from the fluid pressure should equal the actual volume, V, of the pore. This is achieved by augmenting the virtual work expression for the structure with the constraint equation

$$V - \bar{V} = 0 \tag{56}$$

and the total virtual work can be expressed as

$$\delta \Pi^* = \delta \Pi - p \delta V - \delta p (V - \bar{V}) \tag{57}$$

where $\delta \Pi^*$ is the augmented virtual work expression, and $\delta \Pi$ is the virtual work expression for the structure without the fluid phase, $-p\delta V$ is the virtual work contributed by the pore fluid pressure, δp can be regarded as a Lagrange multiplier enforced constraint $V - \bar{V} = 0$. This augmented expression represents a mixed formulation in which the structural displacements and fluid pressure are primary variables.

Once the displacements of solid structure and deformed fluid pressure are solved by the finite element method, we can compute the effective stiffness $\overline{C}_{ijkl}$ of the fluid-filled structure by Eq.(55).

3.2   *Boundary conditions of the RVE subjected to inner pressure*

In contrast to the micromechanical model discussed in Section 2, the initial configuration can be easily obtained by applying internal pore pressure to the fictitious stress-free configuration. By applying an initial pore pressure, the corresponding macroscopic strains of the unit cell are produced in the initial configuration. It is emphasized that the produced initial macroscopic strain is with respect to the fictitious stress-free configuration.

Before applying the fluid pressure in the fictitious stress-free configuration, periodic boundary conditions were applied to the faces of the 3D RVE because the effective behavior derived under these conditions is always bounded by those obtained under internal pressures (Hazanov and Huet, 1994; Khisaeva and Ostoja-Starzewski, 2006).

Let x_1, x_2 and x_3 be the Cartesian coordinates corresponding to axes parallel to the RVE edges as shown in Figure 4. $u(x_1, x_2, x_3)$ is the displacement vector at a point with coordinates (x_1, x_2, x_3). The periodic boundary conditions (PBC) can be expressed in terms of the macroscopic strain $\bar{\varepsilon}_{ij}^0$ induced by the internal pressure,
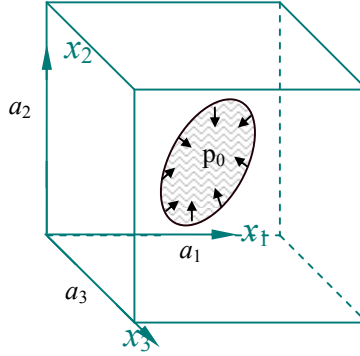
Figure 4: 3-D RVE with initial pore pressure p_0

which stands for the relative strain between opposite faces, as follows

$$
\begin{aligned}
u_i(a_1,x_2,x_3) - u_i(0,x_2,x_3) &= \bar{\varepsilon}_{ij}^0 a_j, && 0 \le x_2 \le a_2, 0 \le x_3 \le a_3 \\
u_i(x_1,a_2,x_3) - u_i(x_1,0,x_3) &= \bar{\varepsilon}_{ij}^0 a_j, && 0 \le x_1 \le a_1, 0 \le x_3 \le a_3 \\
u_i(x_1,x_2,a_3) - u_i(x_1,x_2,0) &= \bar{\varepsilon}_{ij}^0 a_j, && 0 \le x_1 \le a_1, 0 \le x_2 \le a_2
\end{aligned}
\tag{58}
$$

where a_1, a_2 and a_3 are the edge lengths of RVE along x_1, x_2 and x_3 directions, respectively. It is pointed out that the initial macroscopic strain $\bar{\varepsilon}_{ij}^0$ is unknown when the RVE is subjected to an internal pressure. Therefore, the PBCs defined in Eq.(58) cannot be directly applied on the RVE in fictitious stress-free configuration before solving. To describe the boundary conditions of RVE subjected to internal pressure, we eliminate $\bar{\varepsilon}_{ij}^0$ in Eq.(58) and obtain the following boundary conditions for the 3D RVE alternatively,

$$
\begin{aligned}
u_i^{(1)}(a_1,x_2,x_3) - u_i^{(1)}(0,x_2,x_3) &= u_i^{(2)}(a_1,x_2,x_3) - u_i^{(2)}(0,x_2,x_3) = \cdots \\
&= u_i^{(m1)}(a_1,x_2,x_3) - u_i^{(m1)}(0,x_2,x_3) \\
u_i^{(1)}(x_1,a_2,x_3) - u_i^{(1)}(x_1,0,x_3) &= u_i^{(2)}(x_1,a_2,x_3) - u_i^{(2)}(x_1,0,x_3) = \cdots \\
&= u_i^{(m2)}(x_1,a_2,x_3) - u_i^{(m2)}(x_1,0,x_3) \\
u_i^{(1)}(x_1,x_2,a_3) - u_i^{(1)}(x_1,x_2,0) &= u_i^{(2)}(x_1,x_2,a_3) - u_i^{(2)}(x_1,x_2,0) = \cdots \\
&= u_i^{(m3)}(x_1,x_2,a_3) - u_i^{(m3)}(x_1,x_2,0)
\end{aligned}
\tag{59}
$$

where $u^{(m)}$ is the displacement vector of the *mth* node for each face, m_1, m_2 and m_3 are corresponding node numbers at three pairs of faces.

These boundary conditions must be enforced by using coupling constraint equations (CCEs). In the finite element analysis, CCEs are applied between degrees

of freedom (DOFs) in pairs of faces, edges and vertices. From the structure of 3D RVE shown in Figure 4, each common edge belongs to two faces while each corner belongs to three faces. On every edge, each component of displacements would be used to impose two CCEs, one from each face. Similarly, since three faces converge at a vertex, three periodic CCEs, one from each face, need to be imposed using a single component of displacements. Once a DOF has been used in a CCE, it can not be used in another CCE. As a corollary, constraint equations on faces, edges and vertices of the RVE must be applied separately from Eq.(59). Furthermore, only three equations, one for each component of displacement u_i can be written between a pair of faces, edges and vertices.

For the points in three pairs of faces (except points in edges and vertices), CCEs are applied as follows

$$
\begin{aligned}
u_i^{(1)}(a_1,x_2,x_3) - u_i^{(1)}(0,x_2,x_3) &= u_i^{(2)}(a_1,x_2,x_3) - u_i^{(2)}(0,x_2,x_3) = \cdots \\
&= u_i^{(n1)}(a_1,x_2,x_3) - u_i^{(n1)}(0,x_2,x_3) \\
u_i^{(1)}(x_1,a_2,x_3) - u_i^{(1)}(x_1,0,x_3) &= u_i^{(2)}(x_1,a_2,x_3) - u_i^{(2)}(x_1,0,x_3) = \cdots \\
&= u_i^{(n2)}(x_1,a_2,x_3) - u_i^{(n2)}(x_1,0,x_3) \\
u_i^{(1)}(x_1,x_2,a_3) - u_i^{(1)}(x_1,x_2,0) &= u_i^{(2)}(x_1,x_2,a_3) - u_i^{(2)}(x_1,x_2,0) = \cdots \\
&= u_i^{(n3)}(x_1,x_2,a_3) - u_i^{(n3)}(x_1,x_2,0)
\end{aligned}
\tag{60}
$$

where n_1, n_2 and n_3 are corresponding node numbers of three pairs of faces (except points in edges and vertices).

For the points in six pairs of edges (except points in vertices), CCEs are reduced to the following constraint equations (with $i= 1, 2, 3$), as follows,

$$
\begin{aligned}
u_i(x_1,a_2,a_3) - u_i(x_1,0,0) &= u_i(x_1,a_2,x_3) - u_i(x_1,0,x_3) + u_i(x_1,x_2,a_3) \\
&\quad - u_i(x_1,x_2,0) \\
u_i(x_1,0,a_3) - u_i(x_1,a_2,0) &= -u_i(x_1,a_2,x_3) + u_i(x_1,0,x_3) + u_i(x_1,x_2,a_3) \\
&\quad - u_i(x_1,x_2,0) \\
u_i(a_1,x_2,a_3) - u_i(0,x_2,0) &= u_i(a_1,x_2,x_3) - u_i(0,x_2,x_3) + u_i(x_1,x_2,a_3) \\
&\quad - u_i(x_1,x_2,0) \\
u_i(a_1,x_2,0) - u_i(0,x_2,a_3) &= -u_i(x_1,x_2,a_3) + u_i(x_1,x_2,0) + u_i(a_1,x_2,x_3) \\
&\quad - u_i(0,x_2,x_3) \\
u_i(a_1,a_2,x_3) - u_i(0,0,x_3) &= u_i(a_1,x_2,x_3) - u_i(0,x_2,x_3) + u_i(x_1,a_2,x_3) \\
&\quad - u_i(x_1,0,x_3) \\
u_i(a_1,0,x_3) - u_i(0,a_2,x_3) &= -u_i(x_1,a_2,x_3) + u_i(x_1,0,x_3) + u_i(a_1,x_2,x_3) \\
&\quad - u_i(0,x_2,x_3)
\end{aligned}
\tag{61}
$$

Four pairs of corners also need to be constrained simultaneously. For each pair, the corners are located symmetrically with respect to the center of the RVE and the

resulting CCEs are applied as follows,

$$
\begin{aligned}
u_i(a_1,a_2,a_3) - u_i(0,0,0) &= u_i(a_1,a_2,x_3) - u_i(0,0,x_3) + u_i(x_1,x_2,a_3) \\
&\quad - u_i(x_1,x_2,0) \\
u_i(a_1,a_2,0) - u_i(0,0,a_3) &= u_i(a_1,a_2,x_3) - u_i(0,0,x_3) - u_i(x_1,x_2,a_3) \\
&\quad + u_i(x_1,x_2,0) \\
u_i(a_1,0,a_3) - u_i(0,a_2,0) &= u_i(a_1,0,x_3) - u_i(0,a_2,x_3) + u_i(x_1,x_2,a_3) \\
&\quad - u_i(x_1,x_2,0) \\
u_i(a_1,0,0) - u_i(0,a_2,a_3) &= u_i(a_1,0,x_3) - u_i(0,a_2,x_3) - u_i(x_1,x_2,a_3) \\
&\quad + u_i(x_1,x_2,0)
\end{aligned}
\tag{62}
$$

Applying the initial pore pressure in the fluid domain and these three groups of coupling constraint equations on the boundary of solid domain, respectively, we can calculate the initial strain $\bar{\varepsilon}_{ij}^0$ of a unit cell by FEM, then Eqs.(58) can also be determined. Finally, the effective elastic stiffness is obtained with the application of Eq.(55) and note that the applied initial directional strain with respect to the fictitious stress-free configuration is $1 + \bar{\varepsilon}_{ij}^0$.

4 Numerical examples and discussions

In this section several numerical examples are presented to demonstrate the verification, validity and efficiency of these two proposed models. Numerical results obtained are compared with those from other methods available in the literature, and further combined effects of porosity, pore shape, pore pressure and fluid property on the effective properties are investigated.
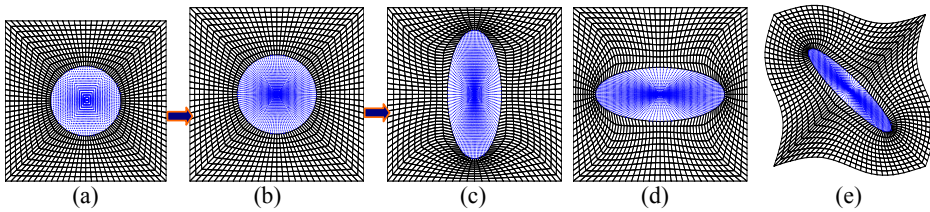

| (a) | (b) | (c) | (d) | (e) |

Figure 5: Deformation configurations of a unit cell with a spherical fluid-filled pore

In the present examples, effective properties of a fluid-filled rock are investigated. The solid was assumed to be isotropic with elastic constants $E_s = 6.0$GPa, $v_s = 0.25$ (Xu, 1998). The pore fluid was assumed to have a bulk modulus of k_f=2.25GPa. The pore shape was chosen as spherical and ellipsoidal, respectively, for the two examples, and the pores were periodically distributed in the solid matrix. Using

the proposed micromechanical model and multiscale homogenization model, we obtained the effective bulk and shear moduli. For the local deformations of unit cell based on the homogenization method, the typical deformation configurations of the central surface of the unit cell with a spherical fluid pore are shown in Fig 5. We applied the initial pore pressure and the corresponding CCEs according to Eqs.(60)-(62) in the fictitious stress-free configuration, and then the initial configuration of the RVE is obtained. Simultaneously, the macroscopic initial strains $\bar{\varepsilon}_{ij}^0$ produced by the inner pressure were computed. To determine effective elastic tensors of unit cell, we further applied the unit initial strain with respect to the initial configuration in every direction and then different current configurations, as depicted in Figs. 5(c)-(e), were determined. Finally the effective elastic tensors were calculated by using Eq.(55) and periodical boundary conditions.
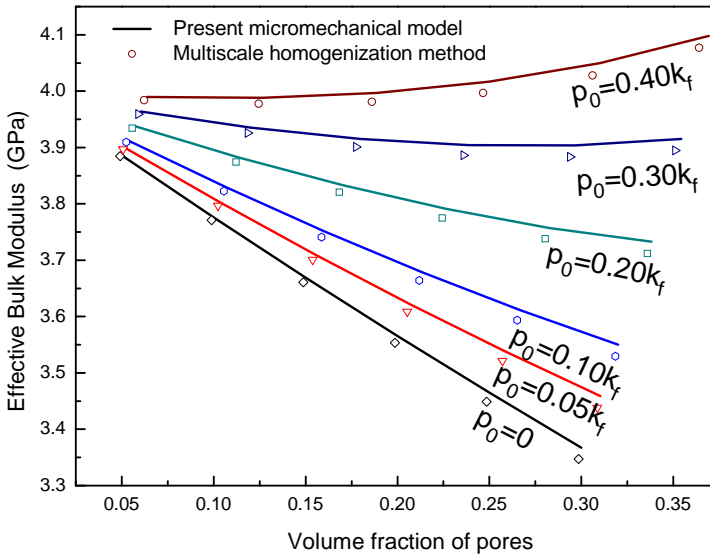

Figure 6: Variations of $\bar{K}$ with pressures and porosities

4.1 *Effects of internal pressures on effective bulk modulus*

For the effective properties of closed cell materials with internal pressure, the variations of effective bulk modulus $\bar{K}$ with initial pressure and porosity are shown in Figures 6-7. As shown in Figure 6, the initial pressure of the fluid can dramatically strengthen the effective bulk modulus. A good agreement is achieved on the results between the micromechanical model and multiscale homogenization model,
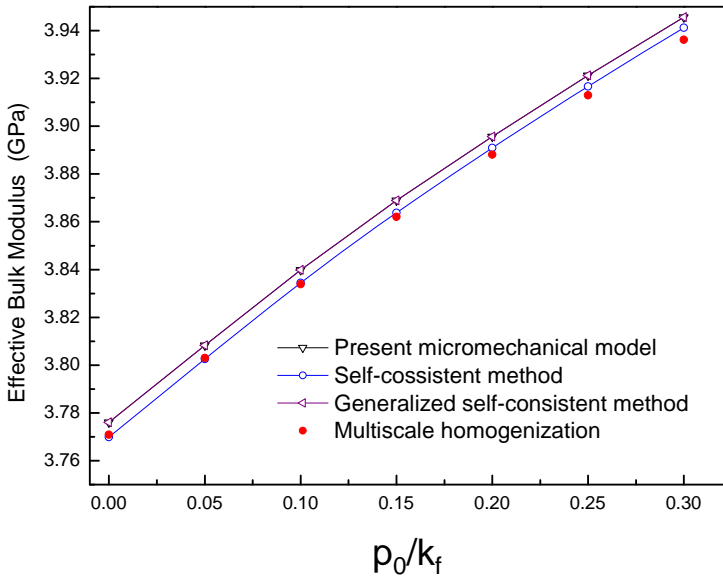
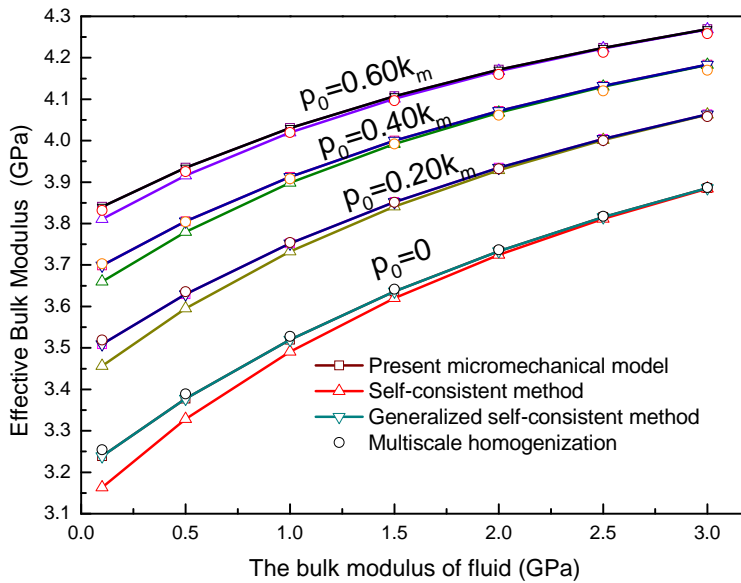Figure 7: Comparisons of different models on fluid bulk modulus and pressure

Figure 8: The dependence of $\bar{K}$ on fluid bulk modulus and pressure

especially when the volume fraction of pores is relatively small. Due to the limitation of the micromechanical model, the differences between the two results are relatively larger in the case of larger porosity. Figure 7 shows the comparisons between the present models and other developed micromechanical models such as the self-consistent and generalized self-consistent methods. The results obtained from the present micromechanical model are very close to those of the generalized self-consistent model, and both of them are a bit higher than those of self-consistent model and the multiscale homogenization model. From Figure 7, we also find that the bulk modulus has a nearly positive linear tendency with the initial pressure.

4.2   *Effects of fluid properties on effective bulk and shear moduli*

For the closed cell material with a constant pore volume fraction ($\phi_f = 10\%$), the variations of effective bulk modulus $\bar{K}$ with fluid bulk moduli and pressures are described in Figure 8. The effective bulk modulus $\bar{K}$ depends on both the initial pressure and the fluid bulk modulus, whereas the effective shear modulus $\bar{G}$ is independent of them. From the comparisons of different models, it is observed that the results of the micromechanical model and generalized self-consistent models agree well with the homogenization-based results. When the fluid bulk modulus is relatively small, the self-consistent method can underestimate the overall bulk modulus.

For the effective shear modulus, the comparisons between other models and the multiscale homogenization model are also shown in Figure 9. Because the fluid pore cannot resist shear deformations, the macroscopic shear modulus decreases when the pore volume fraction increases. The effective shear modulus from the micromechanical model and the generalized self-consistent models are much closer to that from the multiscale homogenization model.

4.3   *Effective properties of fluid-filled materials with ellipsoidal pores*

Consider another example of fluid-filled materials with ellipsoidal pores, on the x_1-x_2-x_3 orthogonal coordinate system, the geometry of fluid pore in the unit cell is analogous to a spheroid with the rotation axis parallel to the x_1-axis. The equation of the spheroid is described by

$$\frac{(x_1)^2}{a} + \frac{(x_2)^2}{b} + \frac{(x_3)^2}{b} \leq 1 \tag{63}$$

where $\alpha = a/b$ is defined as the aspect ratio of the spheroid.

Similar to the first example discussed above, we calculated the effective elastic tensors of the materials with ellipsoidal fluid pores by the present micromechanical model and the multiscale homogenization model. Based on results from the
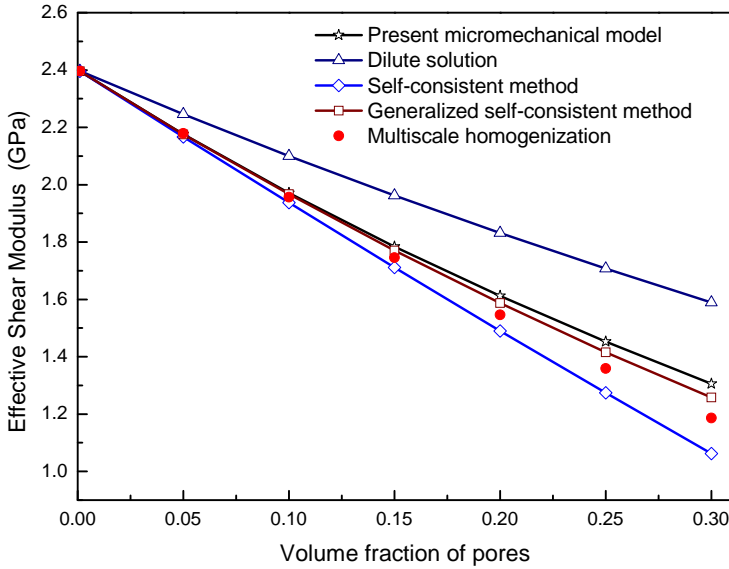
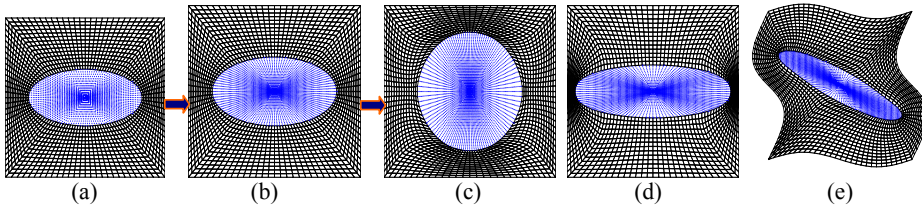Figure 9: Shear modulus $\bar{G}$ by different models

Figure 10: The deformation configurations of central surface of unit cell with an ellipsoidal fluid pore

multiscale homogenization model, Figure 10 illustrates the evolution of local deformation configurations of the central surface of the unit cell with an ellipsoidal fluid pore ($\phi_f = 20\%, p_0 = 0.1k_f, \alpha = 2.0$).

The effective elastic coefficients $\overline{C}_{1111}, \overline{C}_{2222}(\overline{C}_{3333})$ of the closed-cell composite against the initial pore pressures p_0 are plotted in Figure 11. It can be seen that effective elastic coefficients $\overline{C}_{1111}$ and $\overline{C}_{2222}(\overline{C}_{3333})$ monotonously increase when the initial pore pressures increase. When the initial pressure p_0 is relatively small, the comparison between $\overline{C}_{1111}$ and $\overline{C}_{2222}(\overline{C}_{3333})$ has a large difference. The larger the initial pressure, the smaller the gap between $\overline{C}_{1111}$ and $\overline{C}_{2222}(\overline{C}_{3333})$, which
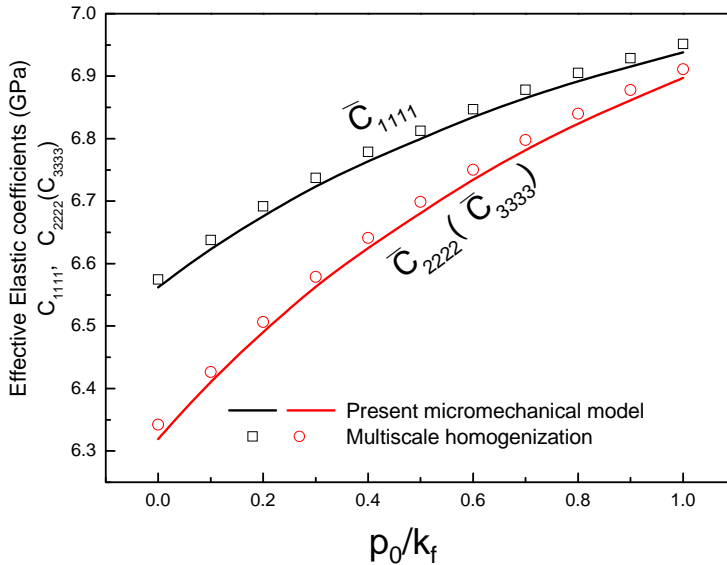
Figure 11: Variations of effective elastic coefficients $\overline{C}_{1111}, \overline{C}_{2222}(\overline{C}_{3333})$ with initial pore pressures

implies that the contribution of p_0 on $\overline{C}_{2222}(\overline{C}_{3333})$ is greater than on $\overline{C}_{1111}$.

For effective shear coefficients, e.g., $\overline{G}_{12}(\overline{G}_{31})$ and $\overline{G}_{23}$, the shear components of effective elastic tensor are independent of fluid properties, and they only depend on the volume fraction of pores. In the case of the aspect ratio of $\alpha = 2$, the relationships between effective shear coefficients and the volume fraction of pores are plotted in Figure 12. The straight line from the Mori-Tanaka model is a slightly higher than the results from the multiscale homogenization model in the case of relatively large pore fraction. It is observed that, with the increasing volume fraction of pores, the effective shear moduli show a negative linear tendency, and the difference between $\overline{G}_{12}(\overline{G}_{31})$ and $\overline{G}_{23}$ becomes larger, which indicates that the apparent anisotropic shear properties are influenced by the presence of ellipsoidal pores.

5 Conclusions

Effective properties of composites with closed cells filled with pressurized fluid are investigated using a micromechanical model and a multiscale homogenization theory. By introducing the configuration variations, the explicit formulations of effective properties with respect to the initial state are derived from the present micromechanical model incorporating the fluid pressure effect. Alternatively, the
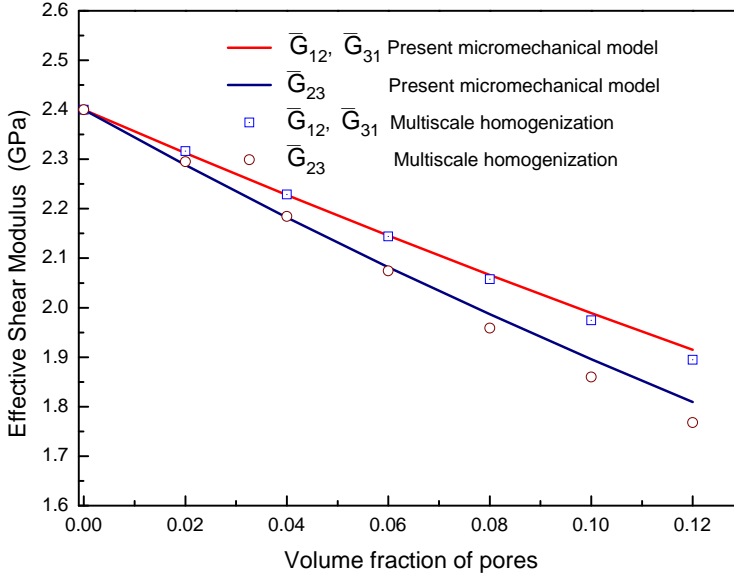
Figure 12: Variations of effective shear moduli $\overline{G}_{12}(\overline{G}_{31}), \overline{G}_{23}$ with volume fractions of pores

multiscale homogenization model, in conjunction with the corresponding boundary conditions, is developed to numerically compute effective moduli of periodic materials by considering the coupling between solid deformations and fluid pressures. Numerical examples are investigated with two types of pore geometries: sphere and ellipsoid, and contributions of the initial fluid pressure in the pores on material properties are incorporated to the proposed models successfully. To verify and validate these two models, the results are compared and a good agreement is found. Further the results show that the fluid pressure within the pores can strengthen the overall bulk modulus, whereas it has no contribution to shear components of the macroscopic elastic tensor due to the inherent characteristics of the fluid and pressure. The strengthen effect of initial fluid pressure on macroscopic bulk modulus can be attributed to the configurations evolution.

The present models can be extended for the determination of effective elasto-plastic behavior of closed-cell porous materials in a nonlinear scope.

6   References

Bakhvalov, N.S.; Panasenko, G.P. (1984): Homogenization in periodic media, mathematical problems of the mechanics of composite materials. Nauka, Moscow.

Benssousan, A.; Lions, J.L.; Papanicolaou, G. (1978): Asymptotic analysis for periodic structures. North-Holland, Amsterdam, The Netherlands.

Biot, M. A. (1954): Theory of elasticity and consolidation for a porous anisotropic solid. *Journal of Applied Physics,* vol. 26, pp. 182-191.

Brown, R.J.S.; Korringa, J. (1975): On the dependence of elastic properties of a porous rock on the compressibility of the pore fluid. *Geophysics* 40, 608-616.

Budiansky, B.; O'Connell, R. (1976): Elastic moduli of a cracked solid. *International Journal of Solids and Structures,* vol. 12, pp. 81-97.

Cheng, L.Y. (1987): Deformation analyses in cell and development biology. Part I-formal methodology. *Journal of Biomedical Engineering,* vol. 109, pp. 10–17.

Christensen, R.M.; Lo, K.H. (1979): Solutions for effective shear properties in three phase sphere and cylinder models. *Journal of the Mechanics and Physics of Solids*, vol. 27, pp. 315-330.

Coussy, O. (1995): Mechanics of Porous Continua. Wiley, New York.

Dormieux, L.; Kondo, D. ; Ulm, F. (2006): Microporomechanics. Wiley, Chichester, England.

Eshelby, J.D. (1957): The determination of the elastic field of an ellipsoidal inclusion, and related problems. *Proceedings of the Royal Society of London*, Series A, 241, pp. 376-396.

Gassmann, F. (1951): Elasticity of porous media. *Vierteljahrschrift der naturforschenden Gesellschaft in Zurich*, vol. 96, pp. 1-21.

Georget, D.M.R.; Smith, A.C.; Waldron K.W. (2003): Modeling of carrot tissue as a fluid-filled foam. *Journal of Materials Science,* vol. 38, pp. 1933-1938.

Gibson, L.J.; Ashby, M.F. (1997): Cullular Solids, Structure and Properteis. Cambridge University Press, Cambridge, UK.

Haasemann, G.; Kastner, M.; Ulbricht, V. (2006): Multi-scale modelling and simulation of textile reinforced materials. *CMC: Computers, Materials and Continua,* vol.3, pp. 131-145.

Hartmann, C.; Delgado, A. (2004): Numerical simulation of the mechanics of a yeast cell under high hydrostatic pressure. *Journal of Biomechanics*, vol. 37, pp. 977-987.

Hartmann, C.; Mathmann, K.; Delgado, A. (2006): Mechanical stresses in cellular structures under high hydrostatic pressure. *Innovative Food Science & Emerging*

Technologies, vol. 7, pp. 1-12.

Hassani, B.; Hinton, E. (1998): A review of homogenization and topology optimization I-homogenization theory for media with periodic structure. *Computers and Structures,* vol. 69, pp. 707-717.

Hazanov, S.; Huet, C. (1994): Order relationships for boundary condition effects in heterogeneous bodies smaller than the representative volume. *Journal of the Mechanics and Physics of Solids*, vol. 42, pp. 1995-2011.

Hill, R. (1965): A self-consistent mechanics of composite materials. *Journal of the Mechanics and Physics of Solids*, vol. 13, pp. 213-222.

Huang, Z.P.; Wang, J. (2006): A theory of hyperelasticity of multi-phase media with surface/interface energy effect. *Acta Mechnica*, vol. 182, pp. 195-210.

Kachanov, M. (1993): Elastic solids with many cracks and related problems. *Advances in applied Mechanics*, vol. 30, pp. 259-445.

Kachanov, M.; Tsukrov, I.; Shafiro, B. (1995): Materials with fluid-saturated cracks and cavities: fluid pressure polarization and effective elastic response. *International Journal of Fracture*, vol. 73, pp. 61-66.

Khisaeva, Z.F.; Ostoja-Starzewski, M. (2006): On the size of RVE in finite elasticity of random composites. *Journal of Elasticity*, vol. 85, pp. 153-173.

Kimmel, E. (1992): Elastic and dissipative moduli of pressure-supported cellular substances. *International Journal of Mechanical Sciences*, vol. 34, pp. 809-815.

Lions, J. L. (1981): Some methods in the mathematical analysis of systems and their control. Science Press, Beijing.

Mori, T.; Tanaka, K. (**1973**): Average stress in matrix and average elastic energy of materials with misfitting inclusions. *Acta Metallurgica*, vol. 21, pp. 571-574.

Nilsson, S. B.; Hertz, C. H.; Falk, S. (1958): On the relation between turgor pressure and tissue rigidity II. *Physiologia Plantarum,* vol. 11, pp. 818-837.

O'Connell R.J.; Budiansky B. (1974): Seismic velocities in dry and saturated cracked solids. *Journal of Geomechanics Research*. Vol. 79, pp. 5412-26.

Okada, H.; Fukui, Y.; Kumazawa, N. (2004): Homogenization analysis for particulate composite materials using the boundary element method. *CMES: Computer modeling in engineering and sciences,* vol. 5, no. 2, pp. 135–150.

Ozgur, M., Mullen, R.L., Welsch, G. (1996): Analysis of closed cell metal composites. *Acta Materialia.* Vol. 44, pp. 2115-2126.

Shafiro, B.; Kachanov, M. (1997): Materials with fluid-filled pores of various shapes: effective elastic properties and fluid pressure polarization. *International Journal of Solids and Structures,* vol. 34, pp. 3517-3540.

Smith, A.E.; Moxham, K.E.; Middelberg, A.P.J. (1998): On uniquely determining cell-wall material properties with the compression experiment. *Chemical Engineering Science*, vol. 53, pp. 3913-3922.

Stenson, J.D.; Thomas, C.R.; Hartley, P. (2009): Modelling the mechanical properties of yeast cells. *Chemical Engineering Science*, vol. 64, pp. 1892-1903.

Sun L.; Wu Y.M.; Huang Z.P.; Wang J. (2004): Interface effect on the effective bulk modulus of a particle-reinforced composite. *Acta Mechanica Sinica*, vol. 20, pp. 676-679.

Tandon, G. P.; Weng, G. J. (1988): A theory of particle reinforced plasticity. *ASME Journal of Applied Mechanics,* vol. 55, pp. 126-135.

Wang,W.X.; Luo, D.M.; Takao, Y.; Kakimoto, K. (2006): New solution method for homogenization analysis and its application to the prediction of macroscopic elastic constants of materials with periodic microstructures. *Computers and Structures*, vol. 84, pp. 991-1001.

Warner, M.; Thiel, B.L.; Donald, A.M. (2000): The elasticity and failure of fluid-filled cellular solids: Theory and experiment. *Proc Natl Acad Sci U S A.* vol. 97, no. 4, pp. 1370-1375.

Xu, S.Y. (1998): Modelling the effect of fluid communication on velocities in anisotropic porous rocks. *International Journal of Solids and Structures*, vol. 35, pp. 4685- 4707.

Yang, Q.S.; Becker, W. (2004): A comparative investigation of different homogenization methods for prediction of the macroscopic properties of composites. *CMES: Computer Modeling in Engineering and Sciences*, vol. 6, pp. 319-332.

Yang, Q. S.; Liu, B. S.; and Meng, L. T. (2009): A Phenomenological Theory and Numerical Procedure for Chemo-Mechanical Coupling Behavior of Hydrogel. *CMC: Computers, Materials and Continua*, Vol. 12, No. 1, pp. 39-56.

Zhang, H.W.; Lv, J.; Zheng, Y.G. (2010): A new multiscale computational method for mechanical analysis of closed liquid cell materials. *CMES: Computer Modeling in Engineering and Sciences*, vol. 68, pp. 55-93.

Zhang,W. X.; Xu, Z.M.; Wang, T.J.; Chen, X. (2009): Effect of inner gas pressure on the elastoplastic behavior of porous materials: A second-order moment micromechanics model. *International Journal of plasticity*, vol. 25, no. 7, pp. 1231-1252.

Zimmerman, R. (1991): Compressibility of sandstones. Elsevier Science, Amsterdam, The Netherlands.